AIP Advances

A method for the frequency control in time-resolved two-dimensional gigahertz surface acoustic wave imaging

Shogo Kaneko, Motonobu Tomoda, and Osamu Matsuda

Citation: AIP Advances **4**, 017124 (2014); doi: 10.1063/1.4863195
View online: http://dx.doi.org/10.1063/1.4863195
View Table of Contents: http://scitation.aip.org/content/aip/journal/adva/4/1?ver=pdfcov
Published by the AIP Publishing

AIP ADVANCES **4**, 017124 (2014)

A method for the frequency control in time-resolved two-dimensional gigahertz surface acoustic wave imaging

Shogo Kaneko, Motonobu Tomoda, and Osamu Matsuda[a]
Division of Applied Physics, Faculty of Engineering, Hokkaido University, Sapporo, Hokkaido 060-8628, Japan

(Received 26 July 2013; accepted 9 January 2014; published online 22 January 2014)

We describe an extension of the time-resolved two-dimensional gigahertz surface acoustic wave imaging based on the optical pump-probe technique with periodic light source at a fixed repetition frequency. Usually such imaging measurement may generate and detect acoustic waves with their frequencies only at or near the integer multiples of the repetition frequency. Here we propose a method which utilizes the amplitude modulation of the excitation pulse train to modify the generation frequency free from the mentioned limitation, and allows for the first time the discrimination of the resulted upper- and lower-side-band frequency components in the detection. The validity of the method is demonstrated in a simple measurement on an isotropic glass plate covered by a metal thin film to extract the dispersion curves of the surface acoustic waves. [http://dx.doi.org/10.1063/1.4863195]

Controlling acoustic wave propagation in media is a key issue for designing acoustic devices such as filters, waveguides, and resonators. In recent years, phononic crystals and phononic metamaterials, which allow one to tailor the acoustic properties of media,[1–6] extend the design freedom of such devices[7–9] and provide opportunities to explore exotic phenomena, such as negative refraction and super lensing.[10–13] To exploit these applications, basic knowledges on the acoustic wave propagation in media or structures in question are of central importance. One of the efficient ways to obtain these is a transient grating experiments.[14,15] In these experiments, surface acoustic waves are generated using laser-induced gratings with short laser pulses, and their propagation is observed in the time-domain. By varying the grating spacing, one may obtain the dispersion curves for the acoustic waves. The time-resolved imaging of acoustic vibrations or waves is another way to get their information.[16–22] Especially the time-resolved two-dimensional surface acoustic wave (SAW) imaging utilizing optical pump-probe technique has successfully clarified the dispersion curves of the SAWs in anisotropic crystals[23] and phononic crystals[24–27] as well as the negative refraction between the phononic-crystal and ordinary medium.[28] Though the time-resolved two-dimensional SAW imaging has better spatial resolution (down to the diffraction limit) than the grating technique has (several periods of the acoustic wavelength), the frequency resolution for the latter is usually better than that for the former.

In a typical setup of the time-resolved two-dimensional SAW imaging measurement,[20,29] the periodic light pulses (pump light pulses) are focused onto the sample surface to generate the SAWs, and the delayed periodic light pulses (probe light pulses) are focused onto the sample to detect the surface displacement caused by the SAWs. By scanning the relative position of the pump and probe light spots, the two-dimensional imaging of the displacement field is achieved. The delay time between the pump and probe light pulse arrival to the sample surface is typically scanned across the laser repetition period to obtain the time-resolved data. In this measurement, the frequency components of the generated SAWs are practically limited to the integer multiples of the

[a]Electronic mail: omatsuda@eng.hokudai.ac.jp

pulse repetition frequency f_0. The resulted frequency resolution of f_0 may be insufficient for many applications, such as the measurement of resonators with high Q value or the precise determination of the dispersion curves of phononic crystals. Varying the laser repetition rate may be a solution for this problem. In Ref. 30, the laser repetition frequency was varied form 800 MHz to over 1000 MHz, and the resonance of a semiconductor membrane around 19 GHz was studied. However, applying similar technique to lasers with much lower repetition frequency around 100 MHz would be difficult because it requires a large variation of the laser cavity length to cover the broad frequency region. (If one wants to vary the repetition frequency from 50 MHz to 100 MHz, for example, the cavity length of the laser needs to be varied from 3 m to 1.5 m.) Reducing the laser repetition frequency to f_0/n (n is an integer) with a pulse picker may be another solution to this problem, but it would not allow one to select arbitrary repetition frequencies, and it would require a very long optical delay line or a complicated timing control.

The purpose of this paper is to propose an extension of the time-resolved SAW imaging with a periodic light source; it allows to generate and detect SAWs at frequencies other than the integer multiples of the source repetition frequency. The paper gives the theoretical description of the principle of the method, and then the validation of the principle in a simple experiment.

To generate the SAWs at various frequencies, we use an amplitude modulation of the light pulse train at a fixed repetition frequency. It is well known that the frequency spectrum of amplitude modulated pulse train contains the main carrier components, which is at the integer multiples of the repetition frequency, and their sideband components, which are located upper and lower sides of the carrier frequencies separated by the modulation frequency. The SAWs excited by such modulated pulse train show the similar frequency spectrum. Thus the generated SAW frequency can be continuously varied by varying the modulation frequency.

In reality, to detect the relatively small signal caused by the SAW propagation, the modulation technique has been commonly used in the previously reported SAW imaging works; the pump light pulses are modulated at frequency F and a lock-in amplifier is used to extract the modulated component in the detected signal. In this case, the generated (and detected) frequency components are at $nf_0 \pm F$ where n is any integer. It is, however, not straightforward to distinguish the upper sidebands ($nf_0 + F$, USBs) and the lower sidebands ($nf_0 - F$, LSBs). Moreover, usually F has been much lower than f_0 (for example, $f_0 \simeq 80$ MHz and $F \simeq 1$ MHz), and no attention has been paid to distinguish the USB and LSB components. Thus the obtained result has been usually regarded as that for nf_0 in the previous works.

In fact, the time-resolved part of the experimental setup of this method is very similar to that for the time-domain thermoreflectance experiments, and the modulation frequency dependence of the thermoreflectance signal has been extensively studied.[31–34] In the thermoreflectance studies, however, the main interest is on the thermal properties at the modulation frequency and it is not necessary to consider the discrimination of the USBs and the LSBs.

In contrast, below we develop a detection and analysis method for the discrimination of the USBs and the LSBs. To explain the principle of the discrimination, we first need to clarify rigorously what we observe in the pump-probe measurement with a periodic light source. Suppose that a train of light pulses at the repetition frequency f_0 is used for both pumping and probing. The amplitude of pump light pulse train is modulated at the frequency F with a modulator. For the pump-probe measurement, we need a variable delay between the pump and probe light pulse arrival to the sample. This may be done by placing an optical delay line in the pump light path or the probe light path. For a while, we consider the case in which the delay line is placed in the pump light path. We may place the delay line in the upper stream (closer to the laser) or lower stream (closer to the sample) of the modulator. Below we consider the case in which the delay line is placed in the lower stream of the modulator so that the modulation envelope is also delayed along with the delay for the pump light pulses.[35]

The acoustic disturbance, e.g. surface displacement, at the real time t with the pump delay time $-\tau < 0$ is given as

$$u(t, \tau) = \sum_{n \geq 0, l = \pm 1} A_{n,l} \cos[-(n\omega_0 + l\Omega)(t + \tau) + \phi_{n,l}], \quad (1)$$

where $\omega_0 = 2\pi f_0$ and $\Omega = 2\pi F$, n specifies the n-th harmonics of ω_0, and $l = 1$ and -1 for the USBs and LSBs, respectively. $A_{n,l}$ is the amplitude and $\phi_{n,l}$ is the initial phase for the vibration at frequency $n\omega_0 + l\Omega$. The summation excludes $(n, l) = (0, -1)$ throughout this article, since it can be unified into $(n, l) = (0, 1)$. We ignore the carrier components at $n\omega_0$ since they are not detected by the lock-in detection at the later stage.

The acoustic disturbance in Eq. (1) is probed at the sampling rate f_0 by the probe light pulse train, which is regarded as a Dirac comb at repetition frequency f_0 or period $T = 1/f_0$ because the pulse duration (<1 ps) is much shorter than the temporal scale of the variation in u ($\gtrsim 100$ ps). The vibration component at the frequency $n\omega_0 + l\Omega$ in Eq. (1) probed by the N-th pulse of the probe pulse train is expressed as

$$\begin{aligned} u_{n,l,N}(\tau) &= A_{n,l}\cos[-(n\omega_0 + l\Omega)(NT + \tau) + \phi_{n,l}] \\ &= A_{n,l}\cos[-l\Omega NT - (n\omega_0 + l\Omega)\tau + \phi_{n,l}]. \end{aligned} \tag{2}$$

The $u_{n,l,N}(\tau)$ oscillates at Ω in the NT domain (corresponding to the t domain), whereas it oscillates at $n\omega_0 + l\Omega$ in the τ domain.

The signal in Eq. (2) is processed with a lock-in amplifier with a reference signal of non-delayed modulation envelope $\cos \Omega t$. The in-phase output of the lock-in amplifier is given by

$$\begin{aligned} X_{n,l}(\tau) &= \overline{u_{n,l,N}(\tau)\cos(\Omega NT)} \\ &\simeq \frac{A_{n,l}}{2}\cos[-(n\omega_0 + l\Omega)\tau + \phi_{n,l}], \end{aligned} \tag{3}$$

where the overscore expresses the average on N. In this paper, it is defined as

$$\overline{s_N} = \frac{1}{N_{\max}}\sum_{j=0}^{N_{\max}-1} s_j$$

for an arbitrary series s_j ($j = 0, 1, 2, \cdots$) with a sufficiently large number $N_{\max}$ which is determined by the lock-in time constant. Likewise, the quadrature output is given by

$$\begin{aligned} Y_{n,l}(\tau) &= \overline{u_{n,l,N}(\tau)\sin(\Omega NT)} \\ &\simeq l\frac{A_{n,l}}{2}\sin[-(n\omega_0 + l\Omega)\tau + \phi_{n,l}]. \end{aligned} \tag{4}$$

Equations (3) and (4) show that the acoustic vibration in the t domain for (n, l) in Eq. (1) is mapped to the vibration in the τ domain with the identical frequency.

The actual signal obtained on the output of the lock-in amplifier is the superposition of $X_{n,l}(\tau)$ or $Y_{n,l}(\tau)$ for all the possible (n, l) as

$$X(\tau) = \sum_{n,l} X_{n,l}(\tau), \quad Y(\tau) = \sum_{n,l} Y_{n,l}(\tau).$$

To retrieve $A_{n,l}$ and $\phi_{n,l}$ from the experimental results $X(\tau)$ and $Y(\tau)$, it is convenient to define a complex signal

$$Z(\tau) = X(\tau) + iY(\tau) = \sum_{n,l} Z_{n,l}(\tau) \tag{5}$$

with

$$\begin{aligned} Z_{n,l}(\tau) &= X_{n,l}(\tau) + iY_{n,l}(\tau) \\ &\simeq \frac{A_{n,l}}{2}\exp\{il[-(n\omega_0 + l\Omega)\tau + \phi_{n,l}]\}. \end{aligned} \tag{6}$$

If $Z(\tau)$ were available for $-\infty < \tau < \infty$, $A_{n,l}$ and $\phi_{n,l}$ would be obtained through the Fourier transform

$$F_T(\omega) = \frac{1}{2\pi}\int_{-\infty}^{\infty} Z(\tau)\exp(i\omega\tau)d\tau$$
$$= \sum_{n,l}\frac{A_{n,l}}{2}\exp\{il\phi_{n,l}\}\delta(\omega - (ln\omega_0 + \Omega)). \quad (7)$$

The USB ($l = 1$) information is obtained from the Fourier amplitude for $\omega > 0$, whereas the LSB ($l = -1$) information is obtained from that for $\omega < 0$. By virtue of the periodic nature of $Z(\tau)$, however, we only need $Z(\tau)$ for $0 \le \tau < \tau_{\max}$ where both $\omega_0\tau_{\max}$ and $\Omega\tau_{\max}$ are integer multiples of 2π. In this case, $A_{n,l}$ and $\phi_{n,l}$ is obtained through

$$F_T(\omega) = \frac{1}{\tau_{\max}}\int_{0}^{\tau_{\max}} Z(\tau)\exp(i\omega\tau)d\tau$$
$$\simeq \sum_{n,l}\frac{A_{n,l}}{2}\exp\{il\phi_{n,l}\}\delta_{\omega,ln\omega_0+\Omega}. \quad (8)$$

But it can be shown further that the minimum required region for $Z(\tau)$ is $0 \le \tau < T$. To see why, a useful relation is obtained from Eq. (6) as

$$Z_{n,l}(\tau + T) = Z_{n,l}(\tau)\exp\{-il(n\omega_0 + l\Omega)T\}$$
$$= Z_{n,l}(\tau)\exp(-i\Omega T),$$

thus

$$Z(\tau + T) = Z(\tau)\exp(-i\Omega T). \quad (9)$$

This allows $Z(\tau)$ obtained in $0 \le \tau < T$ being extended as much as needed. In this way we can obtain $A_{n,l}$ and $\phi_{n,l}$ for each (n, l) from the experimental results. Paying attention to the order of the delay line and the modulator as well as the appropriate data analysis is important for the correct USB-LSB discrimination.

Above mentioned method can be extended to ease the requirement for the actual measurement as follows. To cover the whole necessary frequency range with the mentioned method, one needs to use a rather broad frequency range of $0 < F \le f_0/2$. It might be difficult for a photodetector having the necessary band width up to $f_0/2$ with enough signal to noise ratio. This difficulty can be removed by using a heterodyne method: the pump and probe light pulses are modulated at different modulation frequencies $F_{\rm pu}$ and $F_{\rm pr}$, respectively, and the difference frequency component at $F_{\rm ref} = F_{\rm pu} - F_{\rm pr}$ is detected with a relatively narrow band width photodetector and a lock-in amplifier. Below we consider the heterodyne setup in which the delay line is placed at the lower stream of the modulator in the probe light path.

The acoustic disturbance in this case is given by

$$u(t) = \sum_{n\ge 0, l=\pm 1} A_{n,l}\cos[-(n\omega_0 + l\Omega_{\rm pu})t + \phi_{n,l}], \quad (10)$$

where $\Omega_{\rm pu} = 2\pi F_{\rm pu}$. The $u(t)$ is probed by the probe pulse train which is modulated at $\Omega_{\rm pr} = 2\pi F_{\rm pr}$ and is then delayed by τ. The (n, l) component in Eq. (10) probed by the N-th pulse of the train is given by

$$u_{n,l,N}(\tau) = A_{n,l}\cos[-(n\omega_0 + l\Omega_{\rm pu})(NT + \tau) + \phi_{n,l}]$$
$$\times\frac{1}{2}\cos(\Omega_{\rm pr}NT)$$
$$= A_{n,l}\cos[-l\Omega_{\rm pu}NT - (n\omega_0 + l\Omega_{\rm pu})\tau + \phi_{n,l}]$$
$$\times\frac{1}{2}\cos(\Omega_{\rm pr}NT). \quad (11)$$

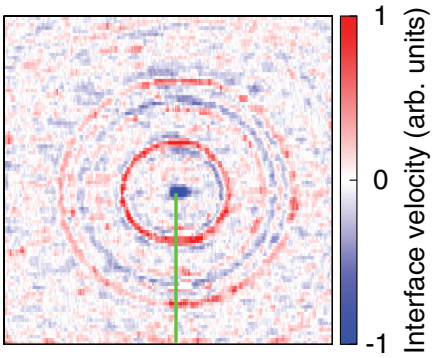

FIG. 1. A snapshot of the SAW propagation over 200 μm×200 μm region with the pump light focused at the center. The dispersion curve is analyzed along the vertical line from the center to the bottom.

The $u_{n,l,N}(\tau)$ is the event observed at the real time $t = NT + \tau$. The factor $\cos(\Omega_{\rm pr} NT)$ is independent of τ since the pulse train is modulated before the delay line. The reference signal for the lock-in detection is $\cos \Omega_{\rm ref} t = \cos[\Omega_{\rm ref}(NT + \tau)]$ with $\Omega_{\rm ref} = 2\pi F_{\rm ref}$. The in-phase lock-in output is given by

$$X_{n,l}(\tau) = \overline{u_{n,l,N}(\tau) \cos[\Omega_{\rm ref}(NT + \tau)]} \simeq \frac{A_{n,l}}{8} \cos[-(n\omega_0 + l\Omega_{\rm pr})\tau + \phi_{n,l}]. \quad (12)$$

Likewise, the quadrature phase output is given by

$$Y_{n,l}(\tau) \simeq l \frac{A_{n,l}}{8} \sin[-(n\omega_0 + l\Omega_{\rm pr})\tau + \phi_{n,l}]. \quad (13)$$

The frequency $n\omega_0 + l\Omega_{\rm pu}$ in the t domain is mapped to the frequency $n\omega_0 + l\Omega_{\rm pr}$ in the τ domain.[36] To retrieve $A_{n,l}$ and $\phi_{n,l}$ from the experimentally obtained $X(\tau)$ and $Y(\tau)$, the Fourier analysis similar to Eqs. (5)–(9) can be used with Ω replaced by $\Omega_{\rm pr}$.

The mentioned heterodyne method is implemented in the time-resolved two-dimensional SAW imaging experiment[29] to demonstrate the validity of the method. For this purpose, a sample having rather simple featureless dispersion relation is used: a crown glass substrate of thickness 1 mm coated with a 40-nm gold film. The light source is a mode-locked Ti:Sapphire laser generating the light pulses of duration ∼100 fs, repetition frequency $f = 75.8$ MHz, and central wavelength 830 nm. The second-harmonic light pulses at wavelength 415 nm are used for pumping, and the light pulses at wavelength 830 nm are used for probing. The pump and probe light pulses are modulated at $F_{\rm pu} = 7.7$ MHz and $F_{\rm pr} = 9.4$ MHz, respectively, by two acousto-optic modulators. The pump light pulses are focused to a ∼2 μm spot on the gold film surface from the film side through a × 50 microscope objective lens to generate the SAWs propagating in all directions with the frequency components up to ∼1 GHz. The modulated probe light pulses are delayed and focused to a ∼2 μm spot on the gold film from the substrate side through another × 50 microscope objective lens to interferometrically detect the resulting out-of-plane Au/substrate interface velocity. The probe light spot position is scanned across the 200 μm×200 μm area of the sample surface. The interferometer output is detected by a photodetector (band width $\lesssim$ 3 MHz) and a lock-in amplifier with a reference signal at $F_{\rm ref} = -1.7$ MHz. We obtain 34 images at regular intervals over the repetition period $T = 13.2$ ns of the laser pulses by scanning the optical delay line which is placed in the probe light path at the lower stream of the modulator.

Figure 1 shows an image of the out-of-plane velocity of the Au/substrate interface at the delay time 11.6 ns. The SAW wavefronts are propagating as concentric circles from the excitation point at the center showing the isotropic nature of the sample.

To get the dispersion curves of the SAWs, the spatiotemporal Fourier transform is performed on the data on the vertical line from the center to the bottom in Fig. 1.[23] For the Fourier analysis, the

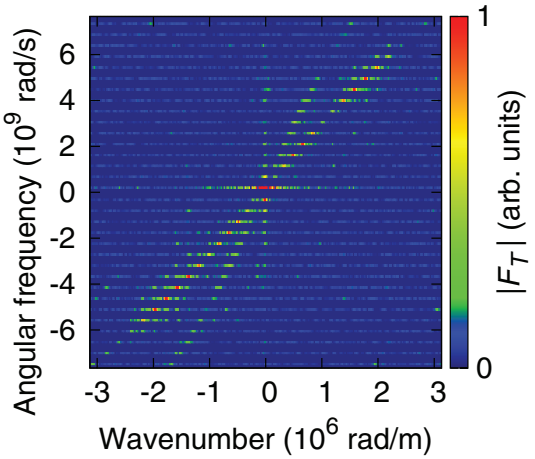

FIG. 2. Modulus of the Fourier amplitude F_T analyzed along the vertical line in Fig. 1 is plotted in the k-ω plane. The positive and negative ω regions correspond to USBs and LSBs, respectively. The finite amplitude in the first and third quadrant indicates the unidirectional propagation of the SAWs in the region of analysis.

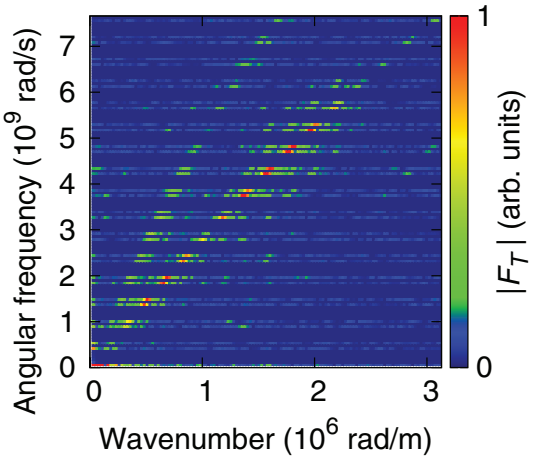

FIG. 3. Modulus of the Fourier amplitude for the USBs and LSBs are plotted together by folding the third quadrant in Fig. 2 onto the first quadrant.

obtained data set for $0 \leq \tau < T$ are extended up to $\tau_{\max} = 8T \simeq 1/F_{\rm pr}$ with Eq. (9). The modulus of the Fourier amplitude $F_T(k, \omega)$ is plotted in the k-ω (wavenumber - angular frequency) plane in Fig. 2. As discussed around Eqs. (7)–(9) and below Eq. (13), the positive ω region corresponds to the USB frequencies, whereas the negative ω region corresponds to the LSB frequencies. Since the SAWs propagate unidirectionally from the center to the bottom in the region of Fourier analysis, the finite Fourier amplitude is observed only in the first quadrant ($k > 0$ and $\omega > 0$) and in the third quadrant ($k < 0$ and $\omega < 0$). To see the USB and LSB results together, the third quadrant is folded onto the first quadrant in Fig. 3. The finite amplitude is observed at the angular frequency $n\omega_0 \pm \Omega_{pr}$ and the peaks for $n\omega_0 + \Omega_{pr}$ (USBs) generally have larger k than those for $n\omega_0 - \Omega_{pr}$ (LSBs).

The points of the local maximum in Fig. 3 are plotted in Fig. 4. The frequencies $n\omega_0 \pm \Omega_{\rm pr}$ in Fig. 3 are remapped to $n\omega_0 \pm \Omega_{\rm pu}$ in Fig. 4. The points represent the allowed SAW modes and are mostly sitting on either of two curves. These can be regarded as the dispersion curves of the SAW modes. The slopes of the branches are estimated as 2870 m/s and 5200 m/s near $k = 0$. They are attributed to the Rayleigh-like waves and the surface skimming longitudinal waves, respectively, as the literature values of the phase velocities of Rayleigh waves and the longitudinal bulk waves are

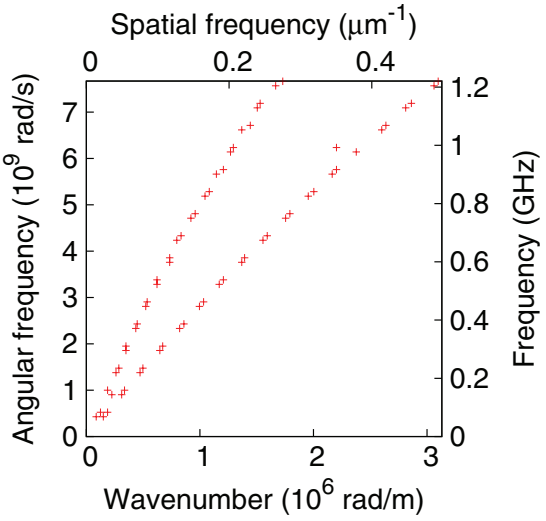

FIG. 4. The points of the local maximum in Fig. 3 are plotted. The frequencies are remapped as in the text. This represents the dispersion curves of the SAW modes.

3130 m/s and 5660 m/s for the crown glass without loading, respectively.[37,38] The pairs of USB and LSB for each integer multiple of f_0 show apparent differences in wavenumbers: the USBs have larger wavenumber values than the corresponding LSBs have. These observations indicate that our mentioned scheme for distinguishing USB and LSB works quite well. Though the measurement is at a single modulation frequency $F_{\mathrm{pu}} = 7.7$ MHz because of the bandwidth limitation of the modulator we used, the method should be valid for whole frequency range $0 < F_{\mathrm{pu}} < f_0/2$ if we use a modulator with faster response, such as an elctro-optic modulator.

In conclusion, we have developed a technique of frequency control in the time-resolved two-dimensional SAW imaging with the pump-probe methods utilizing the modulation of laser pulse trains, the lock-in detection, and the spatiotemporal Fourier analysis. The validity of the proposed method is demonstrated experimentally by the measurement for the crown glass sample. Comparing with the previous time-resolved two-dimensional SAW imaging experiments, the proposed method is advantageous in the freedom of the frequency control. Comparing with the laser-induced grating technique, this method may have a better spatial resolution which is only determined by the diffraction limit. As for the efficiency of the measurement, however, the laser-induced grating technique can obtain the broad frequency band at once for a given grating spacing, whereas the proposed method requires individual measurement for each modulation frequency. Though the proposed method will not replace the existing method entirely, it yet promises versatile application of the SAW imaging technique, for example testing microstructures which possess sharp frequency resonances or complicated dispersion curves. In addition, the method is also applicable to the frequency control in any of pump-probe measurements with periodic excitation, such as those in spintronics and plasmonics.

[1] M. M. Sigalas and E. N. Economou, J. Sound Vib. **158**, 377 (1992).
[2] M. S. Kushwaha, P. Halevi, G. Martínez, L. Dobrzynski, and B. Djafari-Rouhani, Phys. Rev. B **49**, 2313 (1994).
[3] Y. Tanaka and S. Tamura, Phys. Rev. B **58**, 7958 (1998).
[4] J. O. Vasseur, P. A. Deymier, B. Chenni, B. Djafari-Rouhani, L. Dobrzynski, and D. Prevost, Phys. Rev. Lett. **86**, 3012 (2001).
[5] A. Khelif, B. Aoubiza, S. Mohammadi, A. Adibi, and V. Laude, Phys. Rev. E **74**, 046610 (2006).
[6] J. Mei, Z. Liu, W. Wen, and P. Sheng, Phys. Rev. Lett. **96**, 024301 (2006).
[7] F. Wu, Z. Liu, and Y. Liu, Phys. Rev. E **69**, 066609 (2004).
[8] J. O. Vasseur, P. A. Deymier, B. Djafari-Rouhani, Y. Pennec, and A.-C. Hladky-Hennion, Phys. Rev. B **77**, 085415 (2008).
[9] R. H. Olsson III and I. El-Kady, Meas. Sci. Technol. **20**, 012002 (2009).
[10] S. Yang, J. H. Page, Z. Liu, M. L. Cowan, C. T. Chan, and P. Sheng, Phys. Rev. Lett. **93**, 024301 (2004).
[11] X. Zhang and Z. Liu, Appl. Phys. Lett. **85**, 341 (2004).
[12] S. Guenneau, A. Movchan, G. Pétursson, and S. A. Ramakrishna, New. J. Phys. **9**, 399 (2007).

[13] M. Ambati, N. Fang, C. Sun, and X. g. Zhang, Phys. Rev. B **75**, 195447 (2007).
[14] A. A. Maznev, K. A. Nelson, and J. A. Rogers, Opt. Lett. **23**, 1319 (1998).
[15] A. A. Maznev, O. B. Wright, and O. Matsuda, New. J. Phys. **13**, 013037 (2011).
[16] J. W. Dally, Exp. Mech. **20**, 409 (1980).
[17] R. E. Vines, M. R. Hauser, and J. P. Wolfe, Z. Phys. B **98**, 255 (1995).
[18] J. V. Knuuttila, P. T. Tikka, and M. M. Salomaa, Opt. Lett. **25**, 613 (2000).
[19] M. Clark, S. D. Sharples, and M. G. Somekh, J. Acoust. Soc. Am. **107**, 3179 (2000).
[20] Y. Sugawara, O. B. Wright, O. Matsuda, M. Takigahira, Y. Tanaka, S. Tamura, and V. E. Gusev, Phys. Rev. Lett. **88**, 185504 (2002).
[21] A. A. Maznev, A. M. Lomonosov, P. Hess, and A. A. Kolomenskii, Eur. Phys. J. B **35**, 429 (2003).
[22] C. Glorieux, K. Van de Rostyne, J. D. Beers, W. Gao, S. Petillion, N. V. Riet, K. A. Nelson, J. F. Allard, V. E. Gusev, W. Lauriks, and J. Thoen, Rev. Sci. Instrum. **74**, 465 (2003).
[23] Y. Sugawara, O. B. Wright, and O. Matsuda, Appl. Phys. Lett. **83**, 1340 (2003).
[24] D. M. Profunser, O. B. Wright, and O. Matsuda, Phys. Rev. Lett. **97**, 055502 (2006).
[25] D. M. Profunser, E. Muramoto, O. Matsuda, O. B. Wright, and U. Lang, Phys. Rev. B **80**, 014301 (2009).
[26] I. A. Veres, D. M. Profunser, A. A. Maznev, A. G. Every, O. Matsuda, and O. B. Wright, New. J. Phys. **14**, 123015 (2012).
[27] P. H. Otsuka, K. Nanri, O. Matsuda, M. Tomoda, D. M. Profunser, I. A. Veres, S. Danworaphong, A. Khelif, S. Benchabane, V. Laude, and O. B. Wright, Sci. Rep. **3**, 3351 (2013).
[28] B. Bonello, L. Belliard, J. Pierre, J. O. Vasseur, B. Perrin, and O. Boyko, Phys. Rev. B **82**, 104109 (2010).
[29] T. Tachizaki, T. Muroya, O. Matsuda, Y. Sugawara, D. H. Hurley, and O. B. Wright, Rev. Sci. Instrum. **77**, 043713 (2006).
[30] A. Bruchhausen, R. Gebs, F. Hudert, D. Issenmann, G. Klatt, A. Bartels, O. Schecker, R. Waitz, A. Erbe, E. Scheer, J. R. Huntzinger, A. Mlayah, and T. Dekorsy, Phys. Rev. Lett. **106**, 077401 (2011).
[31] D. G. Cahill, W. K. Ford, K. E. Goodson, G. D. Mahan, A. Majumdar, H. J. Maris, R. Merlin, and S. R. Phillpot, J. Appl. Phys. **93**, 793 (2003).
[32] D. G. Cahill, Rev. Sci. Instrum. **75**, 5119 (2004).
[33] Y. K. Koh and D. G. Cahill, Phys. Rev. B **76**, 075207 (2007).
[34] J. Zhu, D. Tang, W. Wang, J. Liu, K. W. Holub, and R. Yang, J. Appl. Phys. **108**, 094315 (2010).
[35] There are other two setups, the delay line in the upper stream of the modulator in the pump light path, and the delay line in the probe light path with the modulator in the pump light path (distinction of upper/lower stream inapplicable). The treatment in Eqs. (1)–(6) needs to be modified appropriately for these cases. The final result is that the acoustic vibrations at frequencies $n\omega_0 \pm \Omega$ in the t domain are mapped into the signals at frequency $n\omega_0$ in the τ domain.
[36] If the delay line is in the lower stream of the modulator in the pump light path, the mapped frequency is $n\omega + l\Omega_{\mathrm{pu}}$. If the delay line is in the upper stream of the modulator in either of the pump or probe light path, the mapped frequency is $n\omega$ for both USB and LSB.
[37] T. Saito, O. Matsuda, M. Tomoda, and O. B. Wright, J. Opt. Soc. Am. B **27**, 2632 (2010).
[38] G. W. C. Kaye and T. H. Laby, *Tables of Physical and Chemical Constants*, 16th ed. (Longman, England, 1995).